Available online at www.sciencedirect.com
ScienceDirect
Fluid Phase Equilibria 255 (2007) 193–199
FLUID PHASE EQUILIBRIA
www.elsevier.com/locate/fluid

High pressure phase equilibria in methane + waxy systems 1. Methane + heptadecane

Jérôme Pauly [a], Joao Coutinho [b], Jean-Luc Daridon [a,*]

[a] *Laboratoire des Fluides Complexes, Université de Pau, BP 1155, 64013 Pau Cedex, France*
[b] *CICECO, Departamento de Quimica da Universidade de Aveiro, 3810-193 Aveiro, Portugal*

Received 5 March 2007; received in revised form 3 April 2007; accepted 5 April 2007
Available online 18 April 2007

Abstract

Fluid–fluid and fluid–solid phase equilibrium were experimentally determined under pressure on the system methane + heptadecane using a full visibility cell. Measurements were performed using the synthetic method on mixtures ranging from pure heptadecane to 99% of methane. The liquid–solid phase transitions were investigated up to 90 MPa and fluid phase boundary was studied in the temperature domain from 293 to 373 K. The appearance of a minimum in the three phase (V–L–S) equilibrium curve is discussed and it is shown that the difference in the solid phase structure and the presence of a solid–solid phase transition do not affect significantly the phase diagram determined.

Keywords: Solid–liquid equilibrium; Wax; Paraffin

1. Introduction

Some deep high pressure and high temperature oil reservoirs, contain high concentrations of heavy paraffins. These heavy compounds, which are soluble in crude oil under reservoir conditions, may crystallise as waxy solid phases when fluid flows out of the reservoir due to changes in both pressure and temperature. These waxes deposit on the wells and pipelines, leading to a reduction of the operating efficiency during the producing life of the well. Various techniques such as pigging (mechanical method used to physically remove wax off the pipe), addition of wax inhibitors or flow improvers, or heating and thermal insulation can be used to prevent wax accumulation and fouling. However, most of these techniques are costly and the first approach to the adequate design of such remedial techniques is to evaluate the wax crystallization conditions. Paraffin precipitation results from the temperature decrease and also from a solvent loss of solvation capacity due to blending of crude oils during transport or to fluid phase separation due to pressure and temperature changes. Although less important than temperature, pressure has also an influence on wax formation conditions [1–3]. In particular, for methane-rich fluids under high pressure–high temperature conditions, the retrograde condensation may sometime cause heavy organic deposition even with fluids with low heavy component content [4–6]. Thus, gas depressurization may increase the wax appearance temperature by as much as 10 K from saturation to atmospheric pressure in some crude oils [5,7]. The consequences of gas dissolution and/or pressure effects on the phase behaviour need to be well known in order to extrapolate to live oils the measurements performed on stock tank oils. In this context, wax appearance temperature has to be measured under high pressure in a representative sample of various reservoirs fluids ranging from light condensate gas to heavy crude oils. However, natural systems are very complex mixtures made up of a multitude of components whose exact composition are not known. In particular, the length of the *n*-paraffin carbon distribution is indefinite as the highest attainable carbon number is generally arbitrarily set by the analytical protocols employed. For that reason it is more appropriate to study the effect of gas dissolution on synthetic waxes whose composition are perfectly defined. To attempt to quantify the light end influence on the phase behaviour of waxy systems we started a systematic study of phase equilibria on binary or pseudo binary systems made up of a gas (or a mixture of gases) and a waxy part composed of a pure paraffin or a mixture of *n*-alkanes. In this work, measurements were

* Corresponding author.
E-mail address: jean-luc.daridon@univ-pau.fr (J.-L. Daridon).

0378-3812/$ – see front matter © 2007 Elsevier B.V. All rights reserved.
doi:10.1016/j.fluid.2007.04.014

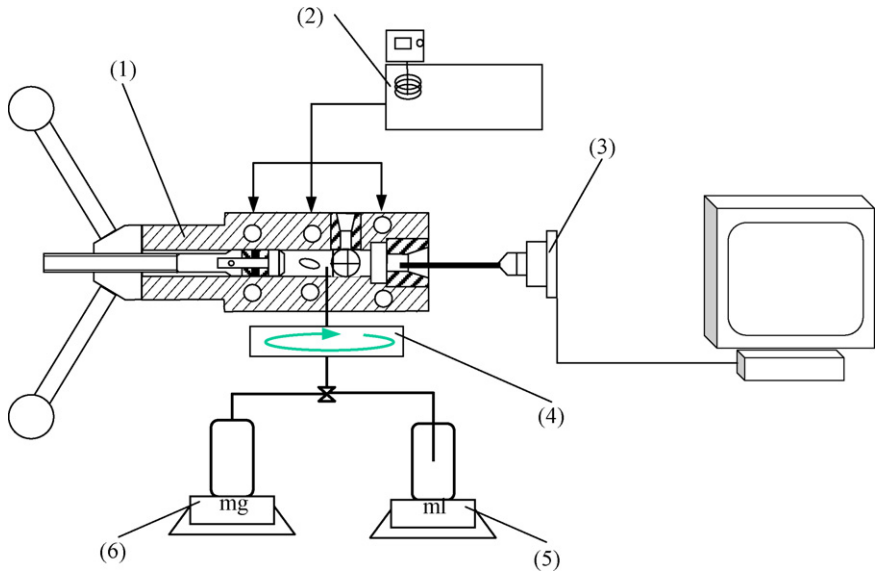

Fig. 1. Schematic diagram of the high pressure apparatus used in this work: (1) high-pressure cell; (2) thermostat bath circulator; (3) endoscope with video camera; (4) magnetic stirrer; (5) liquid weighing; (6) gas weighing.

carried out on the system methane + *n*-heptadecane. A heavy alkane with an odd number of carbon atoms was chosen since mixtures of paraffins crystallise in an orthorhombic structure similar to that presented by pure odd paraffins. A number of binary methane + paraffin systems have been studied previously [8–13] but most of them used paraffins with an even number of carbon atoms. Therefore, the investigation of this system was necessary to evaluate the effect of the crystalline structure on the phase diagram before carrying out studies on complex waxes. The solid–fluid phase transitions were investigated up to 90 MPa and fluid phase equilibria were studied in the temperature region from 283 to 373 K.

2. Experimental

The technique used to measure both fluid–fluid and fluid–solid phase transition is based on a synthetic method which avoids sampling of the phases [10]. The schematic diagram of the apparatus is presented in Fig. 1. The main part of this apparatus is a high pressure cell made of non-magnetic stainless steel. It is closed at one end by a movable piston. The other end is equipped with a sapphire window that allows the visual observation of the entire cell. A second sapphire window is fixed on the cylinder wall in order to light the fluid with an optical fibre. This orthogonal positioning of the light and the observation minimizes the parasitic reflections and improves the observation in comparison to an axial lighting. An image acquisition system made up of an endoscope connected to a video camera is placed behind the sapphire window. This system displays on the screen of a computer the phase transitions which occur in the measuring cell. A small magnetic bar is placed inside the cell allowing the homogenisation of the mixture by means of an external magnetic stirrer. Due to the presence of this magnetic stirring bar as well as of the second window, the minimum internal volume cannot be smaller than 8 cm^3 whereas the maximum volume was fixed to 30 cm^3 in order to limit the size of the cell and thus to reduce thermal inertia and temperature gradients within the cell. The cell temperature is kept constant by circulating a heat-carrier fluid thought three flow lines directly managed in the cell. This heat-carrier fluid is thermo-regulated with temperature stability of 0.01 K by the help of a thermostat bath circulator (HAAKE brand). The temperature is measured with a high accuracy thermometer (AOIP brand) connected to a calibrated platinum resistance inserted inside a well accommodate in the cell close to the sample. The pressure is measured by a piezoresistive silicon pressure transducer (Kulite) placed in contact with the sample in order to reduce the dead volume. As this pressure transducer is placed inside the cell, it is subject to changes of temperature and needs to be calibrated as a function of temperature. This calibration was done in the temperature range 263.15–383.15 K using a dead weight gauge (Budenberg brand) with an accuracy better than 0.02% in the full pressure range (0.1–100 MPa).

The mixtures were directly prepared in the measuring cell. The heavy component was first brought into the cell using vacuum. The exact mass of liquid introduced during this process was determined by weighing by means of precision balance (Ohaus brand) with an accuracy of 10^{-4} g. The methane was then added under pressure. The gas was initially loaded into an aluminium reservoir tank (Gerzat) fixed on the plate of high weight/high precision balance having a maximum weighing capacity of 2000 g with an accuracy of 10^{-3} g (Sartorius) and connected to the measuring cell through a flexible high pressure capillary. The exact mass of gas injected into the measuring cell was determined by weighing the reservoir during the filling of the cell.

Due to super-saturation effects, the phase boundaries were actually evaluated by determining the disappearance conditions of one phase instead of by observation of its appearance. Even if the measurements can be performed either during isothermal or isobaric processes, due to the large slope of the melting

Table 1
Fluid–fluid and fluid–solid phase transitions at a given overall composition (in mol%) of the system methane + heptadecane

T (K)	P (MPa)		T (K)	P (MPa)		T (K)	P (MPa)	
0% of CH_4								
295.35	0.10	L + S → L	299.75	20.8	L + S → L	304.05	40.1	L + S → L
308.30	60.1	L + S → L	312.40	80.1	L + S → L	316.50	99.3	L + S → L
20.21% of CH_4								
292.45	4.09	L + V → L	301.75	4.22	L + V → L	311.25	4.39	L + V → L
322.45	4.57	L + V → L	331.65	4.67	L + V → L	341.55	4.81	L + V → L
351.95	4.93	L + V → L	362.15	5.02	L + V → L	371.15	5.09	L + V → L
293.35	1.82	L + V + S → L + V	292.45	4.09	L + V + S → L + V	293.55	10.01	L + S → L
295.55	19.88	L + S → L	299.65	38.70	L + S → L	303.85	59.32	L + S → L
308.25	78.88	L + S → L						
39.93% of CH_4								
289.95	10.07	L + V → L	293.15	10.25	L + V → L	299.65	10.57	L + V → L
302.85	10.73	L + V → L	313.35	11.14	L + V → L	323.25	11.47	L + V → L
332.75	11.73	L + V → L	342.85	12.03	L + V → L	353.15	12.25	L + V → L
363.15	12.46	L + V → L	372.85	12.66	L + V → L	293.25	2.52	L + V + S → L + V
291.35	5.07	L + V + S → L + V	290.15	7.49	L + V + S → L + V	288.85	10.01	L + V + S → L + V
290.75	19.97	L + S → L	294.55	40.01	L + S → L	298.55	59.72	L + S → L
302.55	79.59	L + S → L						
60.14% of CH_4								
286.45	24.35	L + V → L	289.15	24.39	L + V → L	295.75	24.63	L + V → L
302.55	24.82	L + V → L	313.45	25.13	L + V → L	323.35	25.39	L + V → L
332.95	25.67	L + V → L	343.25	25.89	L + V → L	351.25	26.05	L + V → L
288.85	10.01	L + V + S → L + V	287.15	15.02	L + V + S → L + V	286.65	20.21	L + V + S → L + V
286.45	24.35	L + V + S → L + V	287.25	29.86	L + S → L	289.15	40.50	L + S → L
292.95	59.98	L + S → L	296.65	79.81	L + S → L			
70.40% of CH_4								
286.25	38.48	L + V → L	298.05	37.94	L + V → L	303.15	37.74	L + V → L
314.15	37.44	L + V → L	322.45	37.25	L + V → L	332.15	37.07	L + V → L
341.95	36.95	L + V → L	352.45	36.82	L + V → L	371.15	36.58	L + V → L
286.25	38.48	L + V + S → L + V	287.45	45.19	L + S → L	289.85	60.02	L + S → L
293.05	80.08	L + S → L						
80.09% of CH_4								
287.55	57.99	L + V → L	291.65	57.19	L + V → L	298.65	55.88	L + V → L
303.65	55.24	L + V → L	312.75	54.43	L + V → L	322.75	53.23	L + V → L
332.25	52.36	L + V → L	343.25	51.43	L + V → L	352.05	50.82	L + V → L
362.65	49.91	L + V → L	372.85	49.32	L + V → L	288.35	9.82	L + V + S → L + V
286.35	20.05	L + V + S → L + V	286.15	30.07	L + V + S → L + V	286.25	40.08	L + V + S → L + V
286.55	50.90	L + V + S → L + V	286.80	58.62	L + V + S → L + V	286.95	59.22	L + S → L
287.75	65.13	L + S → L	288.25	69.80	L + S → L	289.05	75.11	L + S → L
290.85	90.06	L + S → L						
88.93% of CH_4								
288.45	74.71	L + V → L	292.25	73.47	L + V → L	303.75	70.18	L + V → L
313.25	68.14	L + V → L	322.25	66.44	L + V → L	332.15	64.68	L + V → L
342.55	63.06	L + V → L	353.25	61.55	L + V → L	363.25	60.05	L + V → L
374.75	58.73	L + V → L	287.65	75.08	L + V + S → L + V	288.05	80.76	L + S → L
288.45	87.12	L + S → L	289.05	95.05	L + S → L			
93.16% of CH_4								
287.85	78.33	L + V → L	289.15	77.73	L + V → L	298.15	74.79	L + V → L
304.25	72.79	L + V → L	313.25	70.78	L + V → L	322.45	68.74	L + V → L
333.55	66.64	L + V → L	343.35	64.85	L + V → L	352.65	63.52	L + V → L
362.15	62.04	L + V → L	287.85	78.26	L + V + S → L + V	288.15	84.35	L + S → L
288.35	90.24	L + S → L						
95.13% of CH_4								
288.05	78.25	L + V → V	291.05	76.89	L + V → V	297.45	74.90	L + V → V
304.75	72.55	L + V → V	312.85	70.56	L + V → V	325.85	67.87	L + V → V
332.65	66.54	L + V → V	341.85	64.79	L + V → V	353.35	62.94	L + V → V
361.15	61.68	L + V → V	370.15	60.22	L + V → V	287.85	78.33	L + V + S → L + V
288.05	85.41	V + S → V	288.15	90.57	V + S → V	288.25	95.62	V + S → V

Table 1 (*Continued*)

T (K)	P (MPa)		T (K)	P (MPa)		T (K)	P (MPa)	
97.47% of CH_4								
287.75	73.76	L + V → V	289.65	73.29	L + V → V	302.45	69.43	L + V → V
311.65	67.28	L + V → V	322.25	64.94	L + V → V	332.65	63.16	L + V → V
342.65	61.31	L + V → V	352.45	59.95	L + V → V	361.65	58.47	L + V → V
287.45	73.47	L + V + S → L + V	287.35	82.88	V + S → V	287.35	87.09	V + S → V
98.03% of CH_4								
287.15	71.27	L + V → V	288.45	70.77	L + V → V	290.55	70.33	L + V → V
302.75	67.19	L + V → V	312.65	64.98	L + V → V	323.65	62.63	L + V → V
332.65	61.05	L + V → V	341.15	59.71	L + V → V	352.75	57.71	L + V → V
360.25	56.71	L + V → V	287.15	71.27	L + V + S → L + V	286.95	80.07	V + S → V
286.75	90.53	V + S → V						
99.12% of CH_4								
286.15	56.84	L + V → V	290.45	55.78	L + V → V	303.65	53.45	L + V → V
313.15	52.12	L + V → V	320.75	51.36	L + V → V	333.15	49.73	L + V → V
342.65	48.28	L + V → V	353.15	47.03	L + V → V	362.95	45.81	L + V → V
286.65	56.83	L + V + S → L + V	285.70	57.50	V + S → V	284.85	60.25	V + S → V
283.85	67.26	V + S → V						

line in the P–T diagram, fluid(s)–solid phase transitions were mostly determined by measuring the solid disappearance temperature at fixed pressure. The experimental procedure was thus performed in two stages. Starting from the fluid(s)–solid phase region, the system is initially heated to approximately determine the temperature of solid disappearance. The system is then cooled again and maintained in fluid(s)–solid equilibrium conditions 2 K below the estimated solid disappearance temperature. The system is then heated stepwise with an increase of 0.1 K every 5 min. As the volume of the sample increases during the melting, the pressure in the system have a tendency to slightly increase during each step. At the end of each step the pressure is reset at the fixed value before a new increment in the temperature in order to stay in an isobaric process. Using this procedure the pressure have fluctuations inferior to 0.1 MPa and the measurements of the fluid (s)–solid phase transition temperatures are repeatable to within 0.2 K. As regards to bubble or dew points determinations, measurements were carried out by observing the pressure disappearance of the vapour or liquid phase at constant temperature. Reproducibility of the pressure disappearance measurements was within 0.05 MPa.

As the minimum volume of the sample is significant, the experimental set-up is not the most appropriate technique to accurately measure the solid–liquid phase transitions of systems without gas solvent due to the thermal inertia of the sample. Therefore, for the pure paraffin, measurements were carried out by means of a microscope equipped with a high pressure cell [14] with an operating range of 0.1–100 MPa. The principle of this apparatus, which has been described in detail in a previous paper [14], consists in the visual observation of the disappearance of the last solid crystal in a thermostated small sample (30 mm^3).

The methane used in this study was supplied by Messer with a guarantee of 99.99% purity. The heptadecane was supplied by Fluka. Its purity was better than 99 mass% and no further purification was carried out.

3. Results and discussion

The system was studied using isoplethic measurements performed on several mixtures with methane content ranging from 0 (pure heptadecane) to 99 mol%. The results are presented in Table 1 along with the nature of the transitions. The three-phase equilibrium conditions were determined by direct observation and checked by recording the intersection of the two-phase boundary curves. The combined data allowed the plotting of the isopleth P–T phase boundary lines shown in Fig. 2 for all the compositions studied.

It can be observed from this figure that the bubble curve corresponding to a methane mol% of 93% merges with the dew points curve for a methane composition of 95%. This means that the liquid–vapour critical points are located between these two phase boundary curves in the studied composition range. It is therefore possible to use these phase boundary measurements to characterize the critical line. The critical line projection in the pressure–temperature diagram is thus plotted along with

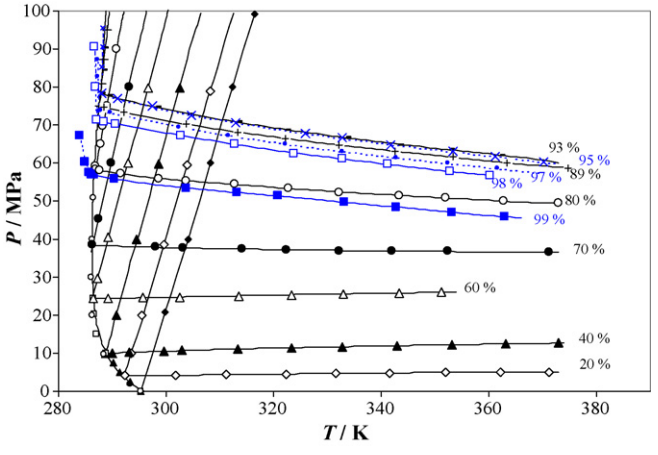

Fig. 2. P–T phase diagram for the various overall compositions studied (in mol% of CH_4). Solid lines bubble points and dashed lines dew points.

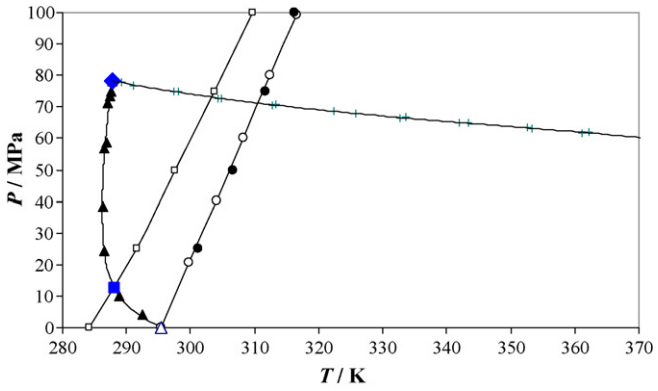

Fig. 3. *P–T* projection of the phase diagram in temperature range investigated. (▲) S + L + V three-phase equilibrium curve; (+) vapour–liquid critical curve; (◯) liquid–solid phase equilibrium line of pure heptadecane measured using microscopy; (●) liquid–solid phase equilibrium line of pure heptadecane measured by Würflinger and Schneider [16]; (□) solid–solid phase equilibrium line of pure heptadecane [16]; (△) triple point of pure heptadecane; (■) quadruple point; (♦) upper critical end point.

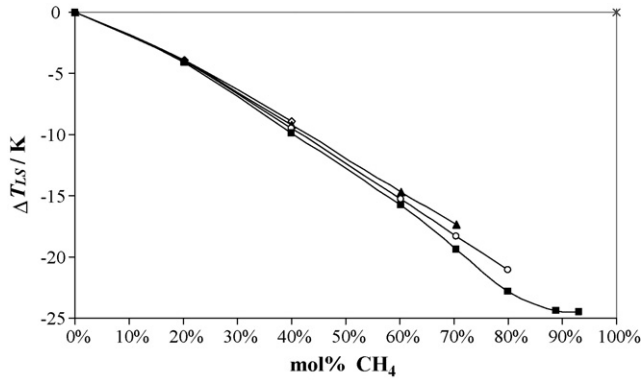

Fig. 4. Difference ΔT_{LS} between the temperature of the onset of crystallisation with (T_{LS}) and without (T^0_{LS}) addition of methane at the same pressure: (◊) 20 MPa; (▲) 40 MPa; (◯) 60 MPa; (■) 80 MPa.

the three-phase equilibrium curve in Fig. 3. Additionally, as pure heptadecane presents one solid–solid phase transition few Kelvin below the melting temperatures [15], both liquid–solid and solid–solid equilibrium lines [16] of *n*-heptadecane were added in Fig. 3 in order to display the full projection of the binary system phase behaviour in the pressure–temperature range of interest. The transition from the low temperature solid phase β_0 (orthorhombic phase) to the high temperature phase β-RI (orthorhombic phase with a rotator state) is an order–disorder transition call rotational transition [12].

This solid–solid equilibrium line intersects the S + L + V three-phase equilibrium curve leading to a quadruple point ($S_{\beta_0} + S_{\beta\text{-RI}} + L + V$) with a variance equal to zero according to the phase rule. The *P–T* conditions of this point can be directly read in Fig. 3 whereas the fixed composition of the liquid phase can be evaluated by interpolation of overall compositions. The coordinates of this point are thus: $T_4 = 288.1$ K, $P_4 = 12.7$ MPa, $X_{CH_4} = 44.7\%$. The existence of this quadruple point does not modify the general shape of the three-phase equilibrium curve as it was already observed by Flöter et al. [12] for the methane + tetracosane binary system.

The S + L + V three phase curve starts from the triple point of the pure heavy component and ends when it intersects the liquid–vapour critical line at the upper critical endpoint ($T_{ucep} = 287.85$ K, $P_{ucep} = 78.3$ MPa). This curve is not monotonic but presents a minimum in temperature T_{min} around 286.2 K for a pressure of 39 MPa. This is a common behaviour for gas + heavy alkane systems that comes from the compensation of the gas solubilisation with pressure and the effect of pressure itself over the solid liquid transition. To separate these two contributions, the influence of gas solubilisation was evaluated by calculating the difference between the temperature of the onset of crystallisation with (T_{LS}) and without (T^0_{LS}) addition of methane at the same pressure:

$$\Delta T_{LS}(P) = T_{LS}(P) - T^0_{LS}(P)$$

for different isobars and for liquid compositions ranging from pure heptadecane to liquid–vapour saturation conditions. The results presented in Fig. 4 for various pressures show that the effect of the gas solubility on the crystallisation temperature decreases monotonically as the methane content increases. This curve is not linear. Its slope has a slight variation with an average of −0.25 K/mol% of methane. Furthermore, it can be noticed that the isobaric curves are roughly superposable for methane contents inferior to 70% (in mol). It appears consequently that the sole effect of methane solubilisation on the onset crystallisation temperature is nearly pressure independent while the mixture stays in the liquid state leading to parallel crystallisation lines in this range of composition. This can be seen in Fig. 5 where the slopes of the crystallisation lines (calculated in the vicinity of the S + L + V three phase) are plotted as a function of composition, the slope remains roughly constant for methane up to 70%, then increases suddenly as the composition becomes close to those of the upper critical endpoint, and even change of sign for higher concentrations corresponding to a gas state. No discontinuity is observed in Fig. 5 around the concentration of the quadruple point. The solid phase transition does not appear to bring a noticeable change on the slope of melting lines. This means that the solid–solid phase transition

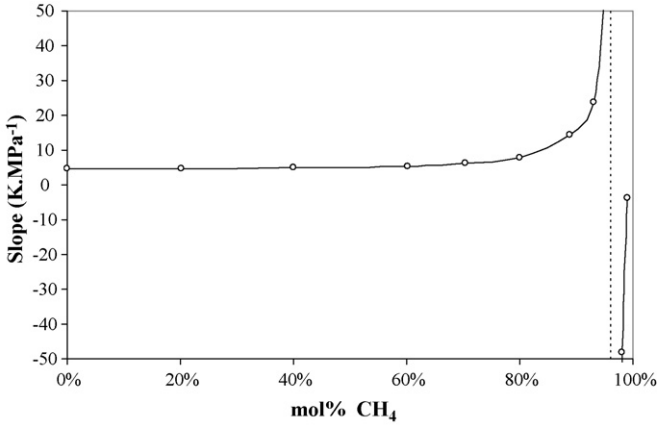

Fig. 5. Slope of the liquid–solid transition line calculated at the S + L + V three-phase equilibrium conditions.

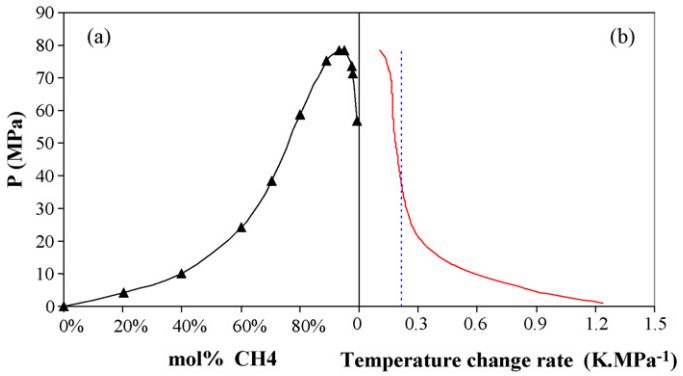

Fig. 6. (a) Liquid composition at the S + L + V three-phase equilibrium conditions. (b) (—) Temperature drop rate due to gas solubilisation; (- - -) pure heptadecane melting slope.

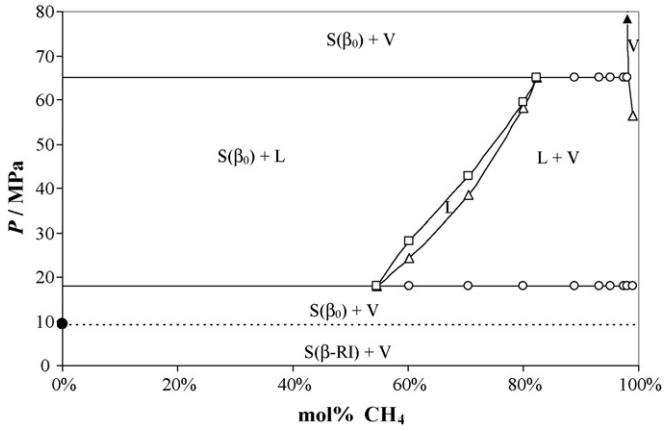

Fig. 8. *P–x* phase diagram at $T = 287$ K.

does not affect substantially the fluid solid phase equilibrium behaviour.

When the system is in three-phase equilibrium, the methane content in the liquid phase is not constant but increases with the pressure (Fig. 6a). This composition change leads to a decrease of the crystallisation temperature that is simultaneously compensated by an increase of the melting temperature of pure heptadecane with pressure (Fig. 7). As it can be observed in Fig. 6b the shape of the temperature drop rate due to the solubilisation of gas is symmetrical to the liquid composition curve. This is a direct consequence of the quasi independence in pressure of the gas solubilisation effect previously observed in Fig. 4. The rate of temperature drop caused by addition of gas to the liquid phase decreases as the pressure increases whereas the pressure effect on pure heptadecane behaviour remains constant leading to a minimum in the three phase line. Thus, the conditions of the minimum are closely linked to the shape of the liquid–vapour phase diagram. This minimum enables the three phase curve to be crossed twice during an isothermal decompression for temperatures ranging from the T_{min} and the melting temperature of pure heptadecane T_m. This means that in this range of temperature solid may form during a decompression.

To be complete, *P–x* curves must be plotted. As phase transitions measurements were not carried out at fixed temperatures, these curves cannot be drawn directly from original data but from interpolated values. The determination of these isotherms was done by correlating the experimental data using low-degree polynomial fits. The numerical values obtained are listed in Table 2 and the phase diagrams are plotted for two isotherms (287 and 290 K) below the triple temperature of the pure heptadecane in Figs. 8 and 9 and for four temperatures above this point in Fig. 10. These diagrams are not complete since the gas composition at low pressures cannot be determined by the synthetic method used in this work as it corresponds to very low solubilities of heptadecane in methane.

At temperatures between the minimum temperature of the three-phase equilibrium curve, T_{min}, and the UCEP, an isotherm intersects the projection of the S + L + V curve in two different points in the *P–T* diagram (Fig. 3). For these temperatures the liquid vapour critical point is glossed over by the solid–fluid transition. It can also be observed in Fig. 8 that this *P–x* diagram only exhibits a small monophasic liquid region enclosed between the liquid–vapour and the liquid–solid two phase domains which intersect each other in two points corresponding to the three-phase equilibrium conditions. As the isotherm 287 K crosses the solid–solid transition line of pure heptadecane

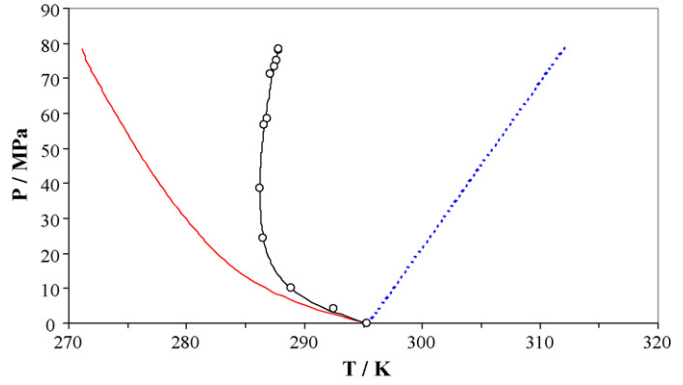

Fig. 7. Separation of contributions in order to explain the presence of a minimum in temperature in the S + L + V three-phase equilibrium curve. (—) Temperature drop due to gas solubilisation; (- - -) liquid–solid phase equilibrium line of pure heptadecane; (◯) S + L + V three-phase equilibrium curve.

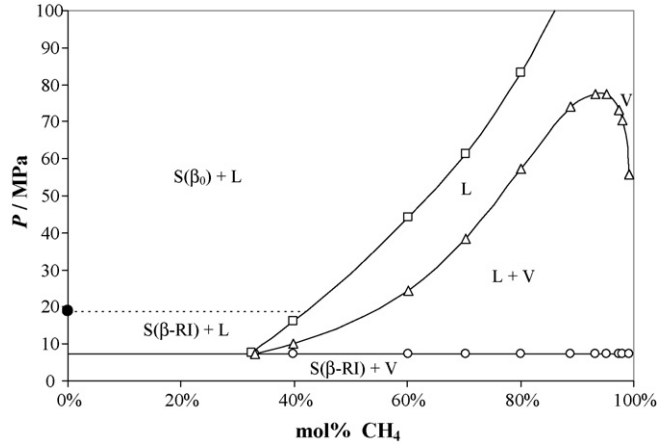

Fig. 9. *P–x* phase diagram at $T = 290$ K.

Table 2
Bubble pressures and dew pressures (in bold) at given compositions and temperatures

mol% of CH_4	P (MPa)								
	287 K	290 K	300 K	310 K	320 K	330 K	340 K	350 K	360 K
20.21			4.20	4.36	4.52	4.66	4.79	4.91	5.00
39.93		10.07	10.59	11.01	11.36	11.67	11.94	12.18	12.40
60.14	24.35	24.44	24.75	25.04	25.31	25.58	25.83	26.03	26.08
70.40	38.44	38.29	37.86	37.54	37.30	37.12	36.97	36.85	36.73
80.09	58.18	57.44	55.76	54.60	53.55	52.58	51.71	50.92	50.15
88.93		74.18	71.17	68.81	66.81	65.06	63.48	61.98	60.53
93.16		77.45	74.12	71.49	69.25	67.26	65.47	63.87	62.38
95.13		**77.32**	**74.00**	**71.29**	**68.99**	**66.99**	**65.18**	**63.49**	**61.86**
97.47		**73.11**	**70.15**	**67.60**	**65.43**	**63.55**	**61.84**	**60.25**	**58.74**
98.03		**70.41**	**67.91**	**65.51**	**63.37**	**61.54**	**59.84**	**58.18**	**56.73**
99.12		**55.86**	**53.97**	**52.60**	**51.37**	**50.11**	**48.75**	**47.38**	**46.13**

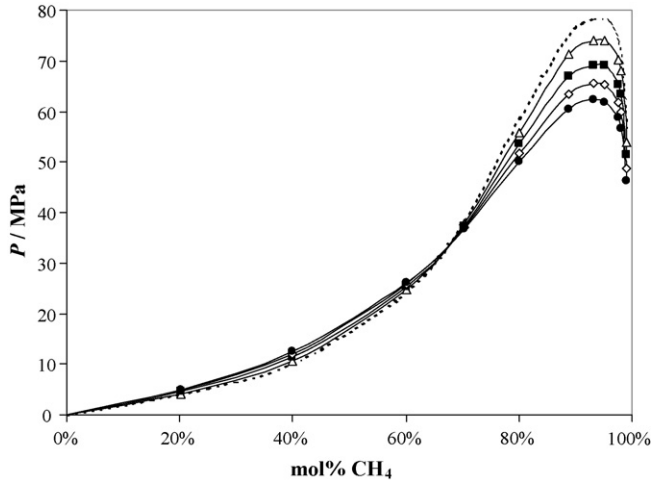

Fig. 10. P–x phase diagram: (△) $T = 300$ K; (■) $T = 320$ K; (◊) $T = 340$ K; (●) $T = 360$ K; (- - -) S + L + V three-phase equilibrium.

below the S + L + V curve another triple line corresponding to the solid $S_{\beta_0} + S_{\beta\text{-RI}} + V$ appears in the diagram. For temperatures between the UCEP and the triple point of pure heavy compounds, an isotherm intersects the projection of the three phase curve in a single point but intersects this time the critical line. The P–x diagram (Fig. 9) is qualitatively similar to the previous in the low pressure region except that solid–solid transition occurs above the S + L + V three phase line. Therefore, the three phase line corresponds to a solid–solid–liquid equilibrium. Once again, nearly no perturbation caused by solid–solid phase transition was observed in this figure on the liquid–solid phase behaviour. At this temperature and at higher pressures the system exhibit a conventional liquid–vapour behaviour since fluid–solid transitions do not interact. For temperatures higher than the triple points, only liquid–vapour equilibria are plotted (Fig. 10) since the solid phase appears only at very high pressures. The different isotherms are very close together and even cross over around 33 MPa and $x_{CH_4} = 67\%$. This behaviour reveals that the isopleths related to low methane content exhibit a slight dependency with temperature in this range. The lower one are increasing whereas above the methane mol% of 67% they are decreasing with the temperature. This behaviour is still observed for the liquid–vapour critical line.

In conclusion the phase diagram of the system methane + heptadecane is qualitatively similar to those of binary mixtures made up of methane plus an heavy alkane with an even number of carbon atoms (C_{16}, C_{20}, C_{22}, C_{24}) previously investigated by de Loos and co-workers [8,10–12]. The difference in the solid phases structure and the presence of a solid–solid phase transition does not affect significantly the phase diagram determined.

References

[1] V. Ruffier Meray, J.L. Volle, C.J.P. Schranz, P. Le Marechal, E. Behar, SPE 26549 (1993) 369–373.
[2] T.S. Brown, V.G. Niesen, D.D. Erickson, SPE 28505 (1994) 415–430.
[3] J.L. Daridon, P. Xans, F. Montel, Fluid Phase Equilib. 117 (1996) 241–248.
[4] P. Ungerer, B. Faissat, C. Leibovici, H. Zhou, E. Behar, G. Moracchini, J.P. Courcy, Fluid Phase Equilib. 111 (1995) 287–331.
[5] J.L. Daridon, J. Pauy, J.A.P. Coutinho, F. Montel, Energy Fuels 15 (2001) 730–735.
[6] M.R. Jensen, P. Ungerer, B. de Weert, E. Behar, Fluid Phase Equilib. 208 (2003) 247–260.
[7] H. Pan, A. Firoozabadi, P. Fotland, SPE Prod. Facil. (1993) 250–258.
[8] M. Glaser, C.J. Peters, H.J. van der Kooi, J. Chem. Thermodyn. 17 (1985) 803–815.
[9] S. Puri, J.P. Kohn, J. Chem. Eng. Data 15 (1970) 372–374.
[10] H.J. van der Kooi, E. Floter, Th.W. de Loos, J. Chem. Thermodyn. 27 (1995) 847–861.
[11] E. Flöter, B. Hollanders, Th.W. de Loos, J. de Swaan Arons, Fluid Phase Equilib. 143 (1998) 185–203.
[12] E. Flöter, Th.W. de Loos, J. de Swaan Arons, Fluid Phase Equilib. 127 (1997) 129–146.
[13] J.J.B. Machado, Th.W. de Loos, Fluid Phase Equilib. 222–223 (2004) 261–267.
[14] J.-L. Daridon, J. Pauly, M. Milhet, Phys. Chem. Chem. Phys. 4 (2002) 4458–4461.
[15] A.-J. Briard, M. Bouroukba, D. Petitjean, M. Dirand, J. Chem. Eng. Data 48 (2003) 1508–1516.
[16] A. Würflinger, G.M. Schneider, Ber. Bun. Ges. Phys. Chem. 77 (1973) 121–128.